Correlations between High-Temperature Oxidation Kinetics and Thermal Radiation Characteristics of Micro-Structured Nickel Surfaces Oxidized at 1173 K

Biying Li [1], Tairan Fu [1],* and Congling Shi [2],*

[1] Key Laboratory for Thermal Science and Power Engineering of Ministry of Education, Beijing Key Laboratory of CO_2 Utilization and Reduction Technology, Department of Energy and Power Engineering, Tsinghua University, Beijing 100084, China; libiying16@mails.tsinghua.edu.cn
[2] China Academy of Safety Science & Technology, Beijing 100029, China
* Correspondence: trfu@mail.tsinghua.edu.cn (T.F.); shicl@chinasafety.ac.cn (C.S.);
  Tel.: +86-10-62786006 (T.F.); +86-10- 84911329 (C.S.)

Abstract: Micro-structured surface functional materials were widely used in electronics, batteries, solar cells, and many other products. However, oxidation at high temperatures greatly affects the material service life and performance. This study focuses on the oxide layer characteristics after high-temperature oxidation and the thermal emissivity of metal materials with micro-structured surfaces. Micro-structured surfaces with various groove morphologies were prepared on 99.9% purity nickel samples. The high-temperature oxidation characteristics of the nickel samples with the microstructure surfaces and the total hemispherical emissivities were measured after various oxidation times in high-temperature (1173 K) air to characterize the correlations between the micro-structure surface oxidization and the emissivity at elevated temperatures. The initial surface roughness greatly affects the surface roughness after oxidation with the oxidation increasing the surface roughness on smooth or less rough surfaces but making the surface smoother for very rough surfaces. The oxidation results show that rougher initial surfaces have larger oxide grain sizes with longer oxidation times leading to smaller grain sizes. The measured total hemispherical emissivity increased with the temperature (500–1400 K) and the oxide layer thickness. The experiments further illustrates that, for the same oxide layer thickness, the measured emissivities become larger for oxides with larger grain sizes caused by the rougher original surfaces. This analysis provides an understanding of the oxidation kinetics of microstructured surfaces and how the oxidized microstructure surfaces affect the thermal radiation properties.

Keywords: high temperature oxidation; microstructured surface; thermal radiation properties

1. Introduction

Mechanical equipment is often operated in high-temperature environments. High-temperature oxidation is then a common cause of corrosion, which strongly influences the properties and service lives of metal materials. Various researchers have attempted to improve the high-temperature oxidation resistance of materials with surface modifications being the most general and intuitive approach, including the application of many kinds of coatings and surface modifications. The oxidation behavior of materials has been widely researched with high-temperature oxidation experiments usually based on Wagner's theory, which is a classic theoretical model. This states that ion diffusion is the key cause of oxidation. Various assumptions and mechanisms have been used to explain oxidation. The oxidation kinetics of metal materials depends on the metal type and the oxidizing conditions. Existing oxidation kinetics models are generally categorized into linear, parabolic, cubic, and logarithmic rate laws.

For example, pure nickel oxidizes very quickly at high temperatures so the initial stage actually manifesting a linear rate controlled by the phase boundary reaction can be ignored. After this very fast initial stake, nickel oxidation is then consistent with the parabolic rate law [1].

Nickel is one of the base metals used in super alloys. Thus, the oxidation behavior of nickel at high temperatures needs to be more fully understood. Geng et al. [2] compared the high temperature oxidation behavior of nickel samples with and without a nanocrystalline layer at 700–900 °C and found that their oxidation rates were the same. Haugsrud [3] studied the effects of surface coatings on the oxidation behavior of nickel by analyzing the relation between the coatings and the outward Ni diffusion. Haugsrud [4] summarized the data and models for the oxidation of nickel at temperatures of 500 to 1400 °C. Zhao et al. [5] investigated the oxidation kinetics, oxide phases, and morphologies of the oxide scales of two Ni-based alloys oxidized at 1050 °C. The results showed that the oxide phases influence the oxidation behavior. Zhou et al. [6] studied the effect of mechanical loadings on the oxidation kinetics of oxide layers on pure Ni oxidized with tensile and compressive stresses at the same temperature. Honvault et al. [7] presented data on the oxidation kinetics of a cermet composed of a Ni-Cu alloy. The mass change was attributed to surface and internal oxidation for some conditions. Wang et al. [8] used a modified phase field approach to investigate the high temperature oxidation behavior of nickel as a function of Young's modulus, COD, and CTE.

The surface thermal radiation properties of high-temperature metal oxides are also important in high temperature applications. For example, Teodorescu et al. [9] studied the spectral-directional emittance of high purity (99.99%) nickel oxidized in air at temperatures between 673 to 873 K. Fu et al. [10–13] measured the total hemispherical emissivity of oxidized nickel at high temperatures using a steady-state calorimetric technique.

There is great interest in using microstructured surfaces to regulate the thermal radiation heat transfer in electronics, materials, and solar energy applications [14–19]. There are some useful ways to improve the micro-structured surfaces [20–22]. Oxidation will always occur on micro-structure surfaces at high-temperature atmosphere environments. High-temperature oxidation studies related to surface structure have mainly used the surface roughness as the primary variable with the oxidation rate investigated by recording the oxidation weight gain. Previous results have indicated that a faster oxidation rate was more likely on rougher surfaces. The oxidized surface morphologies have been analyzed by scanning electron microscopy (SEM) to study the oxidation behaviors for different surface roughnesses [23–29]. In general, the oxide layer on smooth surfaces are relatively uniform and oxide layers more easily form on scratched surfaces for short oxidation times. Oxide layers on rough surfaces are more prone to spall than on smooth surfaces [30]. Furthermore, the surface roughness can also influence the composition of the oxidation products for alloys [31].

High temperature oxidation of microstructured surfaces also affects the thermal radiation characteristics. Most research on high-temperature oxidation has only focused on the effects of temperature, atmosphere, and chemical composition on the oxidation behavior. Further research is needed to describe the effect of oxidation on the thermal radiation characteristics of microstructure surfaces for high temperature oxidation. Little research work has been reported on the correlation between the microstructure surface, oxidation kinetics, and the thermal radiation characteristics at high temperatures [32,33]. Therefore, this work analyzes the oxidation characteristics of microstructured surfaces with various grooved morphologies on pure nickel by analyzing the oxidation layer characteristics and the thermal radiation properties after high-temperature oxidation of nickel samples with various micro-structure surfaces. The results provide a valuable reference for understanding how the oxidized surface micro-structure affects the thermal radiation properties in high-temperature applications.

2. Materials and Methods

Furthermore, 99.9% purity nickel strip samples were prepared. The nickel samples were mechanically polished to mirror finishes with roughnesses of less than 20 nm and then divided

into three groups called S, R1, and R2. The polished samples in group S were retained as the smooth substrates for comparisons. Samples in groups R1 and R2 were ground along the length direction using 1200 grit and 280 grit metallographic sandpapers to form two different rough grooved surfaces. Therefore, the study used nickel samples with different micro-structured surfaces (smooth, shallow grooved rough, and deep grooved rough surfaces) to analyze the surface oxidation behavior at high temperatures.

Samples from the three groups (S, R1, and R2) were cut into smaller strips for high-temperature oxidation experiments to improve the metering accuracy of the electronic balance. The samples were washed with absolute alcohol and then oxidized at 1173 K at an atmospheric pressure and still air in an electric furnace (QSXL-1208, Hangzhou Zhuochi Instrument Co., Ltd., Hangzhou, China). The sample numbers, dimensions, oxidation times, and measurements for the high-temperature oxidation experiments are listed in Table 1.

Table 1. Samples for the high-temperature oxidation tests.

Sample No.		Dimensions (mm × mm × mm)	Oxidation Time (min)	Measurement
S	S0	70 × 10 × 0.2	0	Surface roughness and morphology
	Sox	70 × 10 × 0.2	60	Surface roughness and morphology
	Sm	39 × 10 × 0.2	5–360	Oxidation weight gain
	S-0	270 × 10 × 0.2	0	SEM image and thermal surface radiation property measurements
	S-5	270 × 10 × 0.2	5	
	S-30	270 × 10 × 0.2	30	
R1	R10	70 × 10 × 0.2	0	Surface roughness and morphology
	R1ox	70 × 10 × 0.2	60	Surface roughness and morphology
	R1m	44 × 10 × 0.2	5–360	Oxidation weight gain
	R1-0	270 × 10 × 0.2	0	SEM image and thermal surface radiation property measurements
	R1-5	270 × 10 × 0.2	5	
	R1-30	270 × 10 × 0.2	30	
R2	R20	70 × 10 × 0.2	0	Surface roughness and morphology
	R2ox	70 × 10 × 0.2	60	Surface roughness and morphology
	R2m	39 × 10 × 0.2	5–360	Oxidation weight gain
	R2-0	270 × 10 × 0.2	0	SEM image and thermal surface radiation property measurements
	R2-5	270 × 10 × 0.2	5	
	R2-30	270 × 10 × 0.2	30	

Each group had six samples. The subscript "0" on the sample number represents the un-oxidized sample while the subscript "ox" represents the sample oxidized for 60 min at 1173 K. The surface roughnesses and surface morphologies of the two kinds of samples (subscript "0" and "ox") were examined by a white light interferometer (Contour GT-IM, Bruker, Billerica, MA, USA). The samples (subscript "0" and "ox") were compared for the three surface micro-structures to illustrate how the surface roughness of the oxidized sample is affected by the initial surface condition.

The subscript "m" represents the samples oxidized from 5 to 360 min, which are used to analyze the oxidation weight gain with time using an electronic balance with an accuracy of 0.1 mg.

Additional nickel samples with the three microstructured surfaces (S, smooth, R1, shallow grooved rough, R2, deep grooved rough) were also prepared using the same procedure to study the relationship between the oxidation kinetics of the micro-structured surfaces and the thermal surface emissivity. The sample lengths were increased to 270 mm for the radiation measurements. Two samples in each

group (S, R1, and R2) were oxidized for either 5 or 30 min, which is indicated by the subscripts the samples oxidized for 5 min (samples S-5, R1-5, and R2-5) and for 30 min (samples S-30, R1-30, and R2-30) at 1173 K. Samples S-0, R1-0, and R2-0 were the un-oxidized samples. In total, 10 mm sections of each sample was cut off for the scanning electron microscope (SEM, QUANTA 450 FEG, FEI, Hillsboro, OR, USA) observations to examine the surface morphology. This had no effect on the thermal radiation property measurements.

The total hemispherical emissivities of the samples after oxidization were measured at high temperatures using a steady-state calorimetric measurement apparatus (CMA-1500, Tsinghua University, Beijing, China) [10]. Each sample strip was placed in a cylindrical vacuum chamber (the pressure was less than 0.01 Pa) for the measurements to avoid additional oxidization of the samples in the high-temperature measurements. The emissivities were determined by assuming that each sample was a small body in a large absorbing surface in a vacuum environment. The sample was then electrically heated to the desired temperature. The total hemispherical emissivity of each high-temperature sample was then calculated using the measured heating power through the sample with the surface temperature distribution calculated assuming a steady state. The experiment apparatus and measurement method were described in detail by Fu et al. [10].

3. Results and Discussion

3.1. Oxidation Behavior

The initial average surface roughnesses of the un-oxidized nickel samples (S0, R10, and R20) with the three microstructured surfaces (smooth, shallow grooved rough, deep grooved rough) were measured using the white light interferometer as Ra (S0) =1 4.5 nm, Ra (R10) = 98.9 nm, and Ra (R20) = 605 nm. The larger the surface roughness is, the larger the specific surface area of oxidation will be. In the process of oxidation, the significant microstructure on the surface, as a channel for oxygen atoms to diffuse into the metal, may aggravate the internal oxidation of the metal. The samples after oxidation for 60 min at 1173 K had very different average surface roughnesses of 117 nm, 193 nm, and 428 nm for samples Sox, R1ox, and R2ox, which is shown in Figure 1. Thus, the oxide thicknesses after 60 min oxidation were very different from the original nickel surface roughnesses, so the surface roughnesses of the oxidized samples reflect the oxide layer roughness instead of the nickel substrate roughness. In addition, the rougher initial surfaces of the un-oxidized samples had rougher oxide layers after the oxidation.
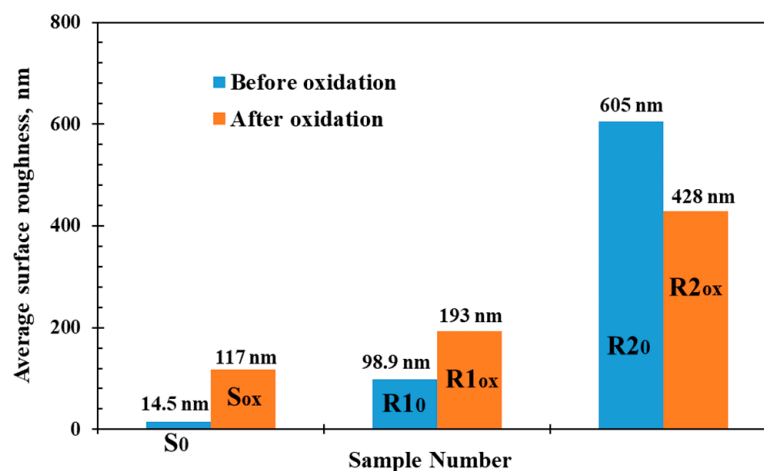

Figure 1. Average surface roughnesses of the nickel samples before and after oxidation for 60 min.

The surface roughnesses before and after oxidation shown in Figure 1 show that the average surface roughnesses of the smooth nickel sample and the shallow grooved rough surface increased greatly after oxidation for 60 min. However, the average surface roughness of the deep grooved

rough surface decreased after oxidation. Thus, the results show that the initial surface roughness affects the surface roughness after oxidation, but in different ways. For smooth or less rough surfaces, the high-temperature oxidation enhances the surface roughness with a rougher oxide layer formed on the sample surface. For rougher surfaces, the high-temperature oxidation makes the surface smoother. The different roughness of the oxide layer formed on micro-structured surfaces reflects, to some extent, the coupling state of compressive stress and tensile stresses within the oxide-metal and oxide-air interfaces.

Figure 2 shows the weight gain per unit area, Δm, during the isothermal oxidation of nickel for various oxidation times, τ, from 5 to 360 min oxidized in air at 1173 K with the data shown as a function of the square root of the oxidation time $\tau^{1/2}$. The growth kinetic rates showed a rapid increase during an initial oxidation time under the effect of molecular oxygen migration and then it begins to slow down to the steady-state rate. The mass increase is almost linearly related to $\tau^{1/2}$, which shows that the growth kinetics are parabolic with a parabolic rate constant based on Wagner's theory. This agrees well with previous experiments [13]. The linear relationship applies for all three surfaces with the various initial surface roughnesses. The slopes in Figure 2 represent the parabolic rate constants for the oxide growth with increases with the initial surface roughness. At higher temperatures, the bulk diffusion determines the oxidation rate. The rougher the metal surface, the larger the oxidation specific surface area, which will make more oxygen diffuse into the metal matrix and increases the occurrence of phase boundary reactions. In addition, a compact oxide layer cannot easily form on the rougher surface as the oxidation begins. These factors result in higher oxidation rates on the rough surface than on the smooth surface since many nucleation sites are available at short oxidation times. Thus, the surface roughness increases the parabolic rate constant for the oxidation of nickel, as shown in Figure 2. The oxide scale thickness may be obtained using the relationship that a mass gain of 0.145 mg/cm^2 corresponds to a 1.0 μm thick oxide film based on data in Figure 1 [30]. The oxide thickness rapidly increases initially and then increases linearly with the oxidation time. At the initial oxidation time of 5 min, the oxide scale thickness is over 1.2 μm larger than the substrate roughness so that the oxide layer can cover the substrate surface. When the oxidation time reached 360 min, the oxide thicknesses of samples Sm, R1m, and R2m, respectively, increased to 7.47, 9.38, and 10.64 μm.
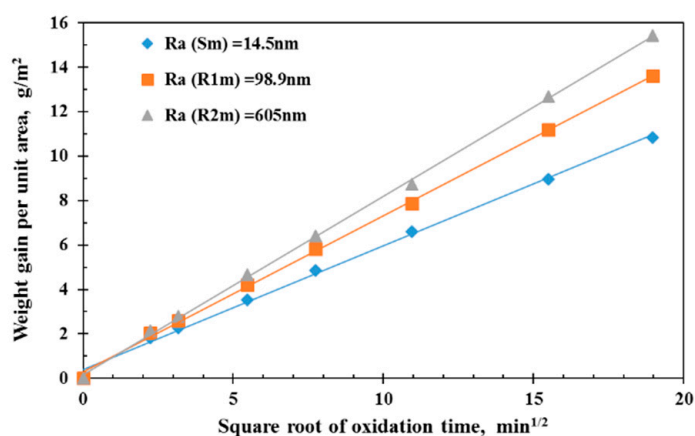

Figure 2. Weight gain per unit area as a function of the square root of the oxidation time on nickel oxidized in air at 1173 K.
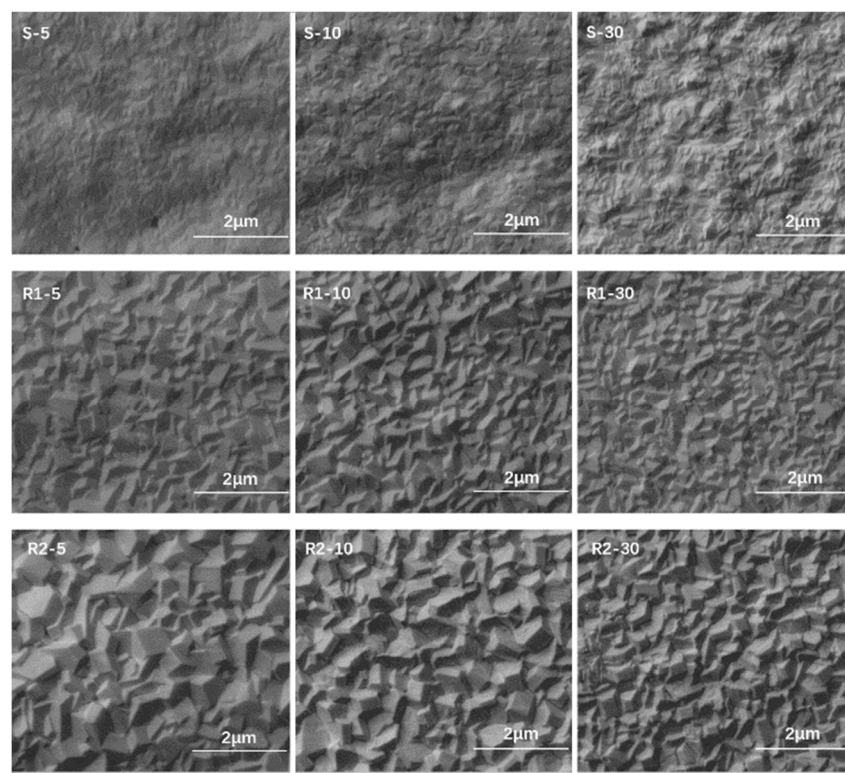
SEM images of the surface morphology of the un-oxidized samples and the samples oxidized for 5, 10, and 30 min from each group (S, R1 and R2) are shown in Figure 3. It is also observed that the smooth surface (group S) becomes rougher, while the roughest surface (group R2) becomes a little smoother after oxidation. Figure 4 shows magnified images of the oxidized surfaces in Figure 3. The oxidized surfaces exhibit ridge-like morphologies. The oxide grain structures with the polygons are larger with relatively clear boundaries for the rough samples from group R1 and R2, but are rounder

for the smooth sample from group S. The phenomenon mechanism can be explained that the stress produced during the oxide formation inside the scale results in the ridges formed on grain boundaries of the surface. The plastic deformation squeezes the oxide layer into the ridges. The amount of ridges decreases when increasing the surface roughness, and the stresses usually increases during the oxide growth so that the amount of surface ridges increases.
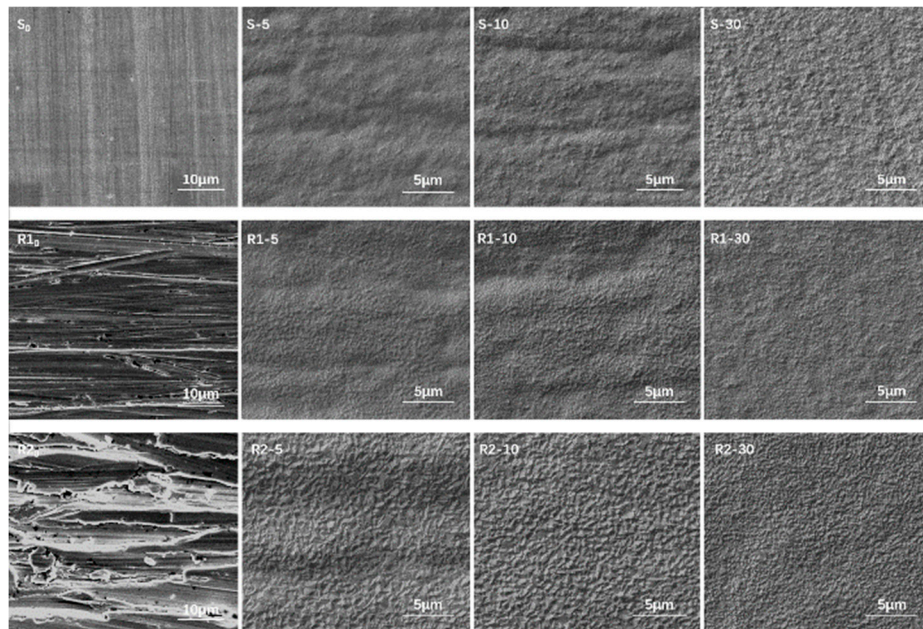
Figure 3. SEM images of the surface morphology of samples oxidized for 0, 5, 10, and 30 min from groups S, R1, and R2.

Figure 4. SEM images of the surface morphology of samples oxidized for 5, 10, and 30 min from groups S, R1, and R2 (magnification of Figure 3).

The pictures in Figure 4 show that the rougher initial surfaces led to larger oxide grains, and longer oxidation times yielded smaller oxide grains. The mechanisms may be suggested to account for the phenomenon. For rougher initial surfaces, the high nucleation rate results in newly generated small embryos that attach to the existing embryos, which increases the embryo size. Once the critical size is exceeded, the embryo growth is accompanied by a reduction of the system-free energy. Embryos spontaneously grow and become stabilized grains that appear larger. However, further oxidation then increases the oxide layer thickness, which hinders the diffusion of ions and reduces the oxidation rate. New embryos are still created on the grain boundaries, but the embryo growth is restrained by the low generation rate. The oxidation grains then get smaller since the slower embryo growth is less likely to become critically-sized embryos in the later stage.

3.2. Thermal Radiation Properties

Nickel samples were again prepared with the various micro-structured surfaces (S, smooth, R1, shallow grooved rough, R2, deep grooved rough). Three samples in each group (S, R1, and R2) were then investigated to analyze the relationship between the microstructure oxidization and the thermal surface emissivity. The sample information is listed in Table 2.

Table 2. Initial surface roughnesses and oxide scale thicknesses of the samples for the emissivity measurements.

Sample No		Oxidation Time/min	Initial Surface Roughness/nm	Oxide Scale Thickness/μm
S	S-0	0	14.5	0
	S-5	5	14.5	1.26
	S-30	30	14.5	2.44
R1	R1-0	0	98.9	0
	R1-5	5	98.9	1.42
	R1-30	30	98.9	2.90
R2	R2-0	0	605	0
	R2-5	5	605	1.48
	R2-30	30	605	3.21

The total hemispherical emissivities of the samples were measured from 500 to 1400 K using a steady-state calorimetric measurement apparatus operated at low pressures [10]. The measured emissivities of the nickel samples from each group oxidized for various oxidation times (corresponding to various oxide layer thicknesses) are compared in Figure 5. The measurement uncertainty for total hemispherical emissivity is within 1.0 to 3.0% [10]. The oxide scale formed on the nickel samples affected the emissivities for all three groups with the measured emissivities increasing with the sample temperature, the oxide layer thickness (Figure 6), and the oxidation time (Figure 7). For example, the emissivity of sample S-0 (un-oxidized smooth surface) increases from 0.092 to 0.186 while the emissivity of sample S-30 (2.44 μm thick oxide layer formed on the smooth surface after oxidation for 30 min) increased from 0.467 to 0.674 when the measurement temperature was increased from 500 to 1400 K. The oxidation scale strongly affects the total hemispherical radiation properties. The emissivity of nickel oxide (dielectric material) is higher than the emissivity of nickel substrate. The thermal radiation emitted by the oxidized nickel sample is the integration of the emitting radiation from the oxide scale and the transmission radiation from the substrate [9,13]. Therefore, the measured total hemispherical emissivity is actually an "apparent" emissivity of the oxidized sample. The increase of the oxide scale thickness will enhance the emittance and attenuate the transmittance of the oxide scale so that the measured apparent emissivity increases with the oxide scale thickness at the same temperature condition. When the oxide scale is thick enough, it can be predicted that the transmission

effect of the substrate may be neglected and the total hemispherical emissivity of the oxidized sample will not vary with the scale thickness.

(**a**) Group S   (**b**) Group R1   (**c**) Group R2
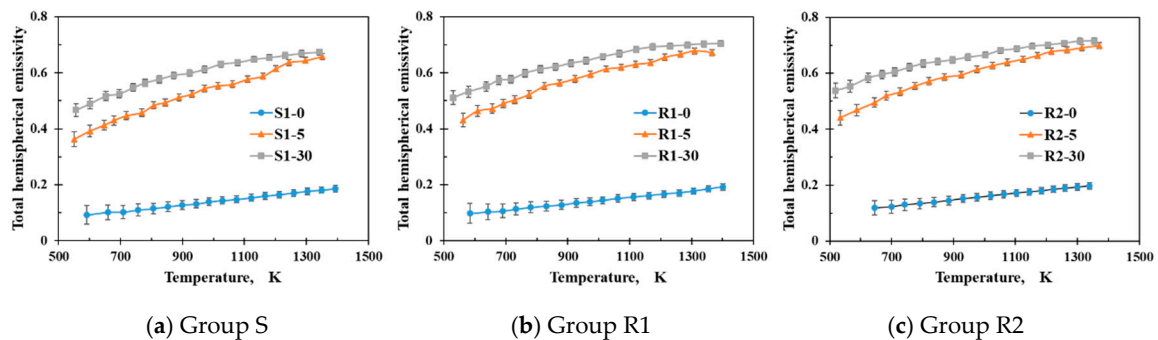
Figure 5. Total hemispherical emissivities as a function of the temperature of samples oxidized for 0, 5, and 30 min based on the initial surface roughness for three groups (S, R1, and R2).

(**a**) Group S   (**b**) Group R1   (**c**) Group R2
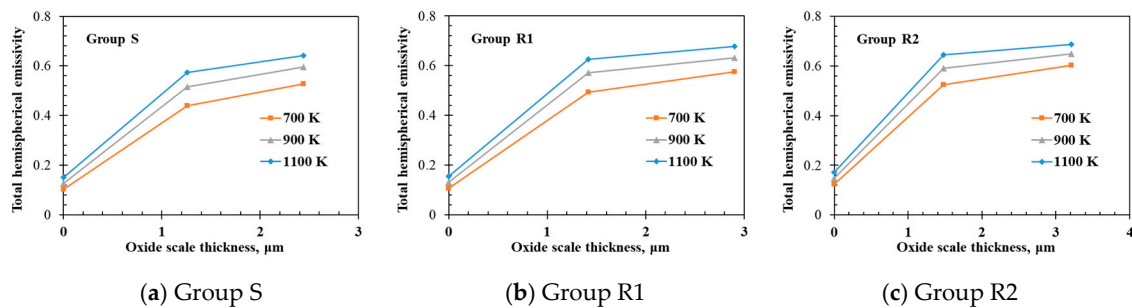
Figure 6. Total hemispherical emissivity as a function of oxide scale thickness at temperatures (700, 900, and 1100 K) for three groups (S, R1, and R2).

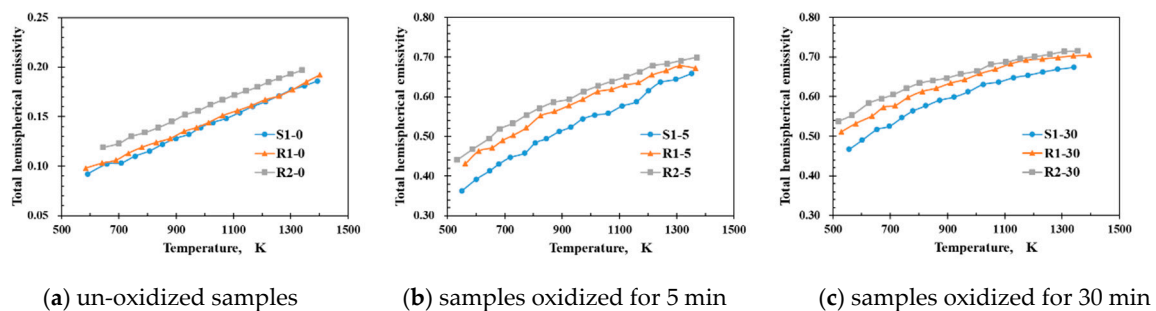(**a**) Group S   (**b**) Group R1   (**c**) Group R2
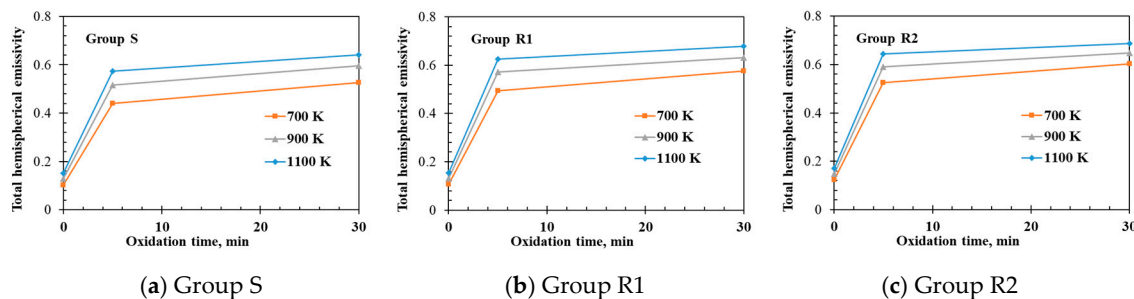
Figure 7. Total hemispherical emissivity as a function of oxidation time at temperatures (700, 900, and 1100 K) for three groups (S, R1, and R2).

The relationship between the surface microstructure and the total hemispherical emissivity is illustrated by comparing the samples with the same oxidation times. Figure 8a shows that the measured emissivities of the un-oxidized samples known as S1-0, R1-0, and R2-0 increase from 500 to 1400 K. The results also illustrate that a large surface roughness increases the specific surface area, so the emissivity should increase. Figure 8b shows the measured emissivities of the samples after being oxidized for 5 min at 1173 K. Their different initial surface roughnesses (14.5, 98.9, and 605 nm) result in different surface roughness characteristics after oxidation, as discussed in Section 3.1 with differing surface microstructures and the layer thicknesses of 1.26, 1.42, and 1.48 μm for samples S1-5, R1-5, and R2-5. Figure 6 shows that a larger initial surface roughness leads to a thicker oxide layer and larger oxide grain sizes, which both increase the surface emissivity. Therefore, the measured total hemispherical emissivity of R2-5 of (0.44, 0.70) for temperatures of 500 to 1400 K is larger than the emissivities of S1-5 (0.36, 0.65) and R1-5 (0.43, 0.67) for the same temperatures. A longer oxidation time at the same oxidation temperature lead to similar relationships between the oxide characteristics and

the emissivity, as shown in Figure 8c, which shows the measured emissivities of samples S1-30, R1-30, and R2-30 after oxidization for 30 min at 1173 K.

(**a**) un-oxidized samples   (**b**) samples oxidized for 5 min   (**c**) samples oxidized for 30 min

Figure 8. Total hemispherical emissivities as a function of the temperature of samples with the various surface microstructures based on the oxidation time for 0, 5, and 30 min.

Thus, the oxide layer thickness and the surface microstructure both affect the total hemispherical emissivity. However, a given sample has only small differences in the surface micromorphology for different oxidation times, as shown in Figure 4. The effect of the surface microstructure after oxidation on the emissivity is illustrated by analyzing the measured total hemispherical emissivity data in Figure 5 to obtain the emissivities at a specified oxide layer thickness and measurement temperature. Table 3 lists the emissivities for the three samples S1, R1, and R2 for an oxide layer thickness of 2.0 μm and an emissivity measurement temperature of 1173 K. The interpolated emissivities of samples R1 and R2, 0.595 and 0.608, are higher than that of group S, 0.566, with little difference between the emissivities for samples R1 and R2. The characteristics can be predicted from the SEM images in Figure 4. The surface micro-morphologies of samples R1 and R2 after oxidation are similar so their emissivities are similar. However, the surface of sample S after oxidation looks very different from the surfaces of samples R1 and R2. Thus, the total hemispherical emissivities of samples R1 and R2 are larger than that of sample S because the oxide layers on nickel samples R1 and R2 have larger grain sizes due to the rougher initial surface. In addition to this factor of the grain sizes, it is also noted that the difference of the substrate emissivities will slightly affect the apparent emissivities.

Table 3. Estimated emissivities of samples S, R1, and R2 for a 2 μm-thick oxide layer and an emissivity measurement temperature of 1173 K.

Group No.	S	R1	R2
Total hemispherical emissivity of un-oxidized substrates	0.160	0.163	0.179
Initial surface roughness/nm	14.5	98.9	605
Oxide scale thickness/μm	2.0	2.0	2.0
Total hemispherical emissivity of oxidized samples	0.566	0.595	0.608

4. Conclusions

The high-temperature oxidation characteristics surface emissivities of nickel samples were investigated for various surface microstructures for various temperatures and oxidation times.

- The results show that rougher initial surfaces of the un-oxidized samples resulted in rougher sample surfaces after oxidation at high temperatures. The initial surface roughness affects the surface roughness after oxidation with the oxidation increasing the surface roughness on smooth or less rough surfaces while making the surface smoother for very rough surfaces.
- SEM images of the oxidized samples show how the nickel oxide grains, especially the grain size, differed for different initial surface roughnesses and different oxidation times with rougher initial surfaces, which leads to larger oxide grain sizes and longer oxidation times leading to smaller grain sizes. These characteristics are consistent with the grain growth mechanism.

- The measured total hemispherical emissivities increased with the sample temperature (500–1400 K) and the oxide layer thickness. The larger surface roughness enhanced the emissivities for the un-oxidized samples. For the oxidized samples, the oxide layers formed on the various sample substrates had different surface microstructures and thicknesses, which affected the total hemispherical emissivity.

- The surface micro-morphologies and the surface emissivities of samples R1 and R2 after oxidation were both similar. However, the surface of sample S after oxidation looked quite different from the surfaces of samples R1 and R2 with the emissivity of sample S after oxidation being lower that the emissivities of samples R1 and R2 because the oxides on samples R1 and R2 had larger grain sizes due to the initially rougher surfaces.

Conflicts of Interest: The authors declare no conflict of interest.

References

1. Birks, N.; Meier, G.H.; Pettit, F.S. *Introduction to the High-Temperature Oxidation of Metals*; Cambridge University Press: Cambridge, UK, 2006; Volume 2013.
2. Geng, S.; Wang, F.; Zhang, S. High temperature oxidation behavior of a sputtered pure Ni nanocrystalline coating at 700–900 °C. *Surf. Coat. Technol.* **2003**, *167*, 212–216. [CrossRef]
3. Haugsrud, R. On the effects of surface coatings on the high-temperature oxidation of nickel. *Corros. Sci.* **2003**, *45*, 1289–1311. [CrossRef]
4. Haugsrud, R. On the high-temperature oxidation of nickel. *Corros. Sci.* **2003**, *45*, 211–235. [CrossRef]
5. Zhao, K.; Zhou, Y.B.; Ma, Y.H.; Lou, L.H.; Hu, Z.Q. Effect of Microstructure on the Oxidation Behavior of Two Nickel-Based Superalloys. *Corrosion* **2005**, *61*, 961–967. [CrossRef]
6. Zhou, C.H.; Ma, H.T.; Wang, L. Comparative study of oxidation kinetics for pure nickel oxidized under tensile and compressive stress. *Corros. Sci.* **2010**, *52*, 210–215. [CrossRef]
7. Honvault, C.; Peres, V.; Cassayre, L. Oxidation kinetics of a Ni–Cu based cermet at high temperature. *Corros. Sci.* **2013**, *68*, 154–161. [CrossRef]
8. Wang, C.; Ai, S.; Fang, D. Effect of Oxidation-Induced Material Parameter Variation on the High Temperature Oxidation Behavior of Nickel. *Acta Mech. Solida Sin.* **2016**, *29*, 337–344. [CrossRef]
9. Teodorescu, G.; Jones, P.D.; Overfelt, R.A.; Guo, B.J. High temperature spectral-directional emittance of high purity nickel oxidized in air. *J. Mater. Sci.* **2006**, *41*, 7240–7246. [CrossRef]
10. Fu, T.R.; Tan, P.; Pang, C.H. A steady-state measurement system for total hemispherical emissivity. *Meas. Sci. Technol.* **2012**, *23*, 025006. [CrossRef]
11. Fu, T.R.; Tan, P. Transient calorimetric measurement method for total hemispherical emissivity. *Trans. ASME J. Heat Transf.* **2012**, *134*, 111601. [CrossRef]
12. Fu, T.R.; Tan, P.; Zhong, M.H. Experimental research on the influence of surface conditions on the total hemispherical emissivity. *Exp. Therm. Fluid Sci.* **2012**, *40*, 159–167. [CrossRef]
13. Fu, T.R.; Tan, P.; Ren, J.; Wang, H.S. Total hemispherical radiation properties of oxidized nickel at high temperatures. *Corros. Sci.* **2014**, *83*, 272–280. [CrossRef]
14. Fukumoto, S.; Takahara, J.; Takahara, J.; Kobayashi, T. Narrow-band thermal radiation by resonant modes inside tungsten microcavities. In Proceedings of the International Quantum Electronics Conference (IQEC), San Francisco, CA, USA, 21 May 2004; pp. 427–429.
15. Huang, J.G.; Xuan, Y.M.; Li, Q. Investigation on emissive properties of peroskite-type oxide LSMO with grating surface. *Sci. China Technol. Sci.* **2011**, *54*, 220–225. [CrossRef]

16. Yin, H.X.; Zhu, C.R.; Shen, Y.; Yang, H.F.; Liu, Z.; Gu, C.Z.; Liu, B.L.; Xu, X.G. Fabrication of large-scale spherical-cap structure and the application on n-GaN based light-emitting diodes. *J. Vacuum Sci. Technol. B Microelectron. Nanometer Struct.* **2014**, *32*, 031208. [CrossRef]

17. Lin, C.; Povinelli, M.L. Optical absorption enhancement in silicon nanowire arrays with a large lattice constant for photovoltaic applications. *Opt. Express* **2009**, *17*, 19371–19381. [CrossRef] [PubMed]

18. Chattopadhyay, S.; Huang, Y.F.; Jen, Y.J.; Ganguly, A.; Chen, K.H.; Chen, L.C. Anti-reflecting and photonic nanostructures. *Mater. Sci. Eng. R Rep.* **2010**, *69*, 1–35. [CrossRef]

19. Li, Y.; Zhang, J.; Yang, B. Antireflective surfaces based on biomimetic nanopillared arrays. *Nano Today* **2010**, *5*, 117–127. [CrossRef]

20. Lamikiz, A.; de Lacalle, L.N.L.; Sanchez, J.A.; Bravo, U. Calculation of the specific cutting coefficients and geometrical aspects in sculptured surface machining. *Mach. Sci. Technol.* **2005**, *9*, 411–436.

21. Arizmendi, M.; Campa, F.J.; Fernández, J.; de Lacalle, L.N.L.; Gil, A.; Bilbao, E.; Veiga, F.; Lamikiz, A. Model for surface topography prediction in peripheral milling considering tool vibration. *CIRP Ann. Manuf. Technol.* **2009**, *58*, 93–96. [CrossRef]

22. De Lacalle, L.N.L.; Rodríguez, A.; Lamikiz, A.; Celaya, A.; Alberdi, R. Five-Axis Machining and Burnishing of Complex Parts for the Improvement of Surface Roughness. *Mater. Manuf. Process.* **2011**, *26*, 997–1003. [CrossRef]

23. Zhang, Y.F.; Shores, D.A. Cracking and Spalling of Oxide Scale from 304 Stainless-Steel at High-Temperatures. *J. Electrochem. Soc.* **1994**, *141*, 1255–1260. [CrossRef]

24. Huntz, A.M.; Lefevre, B.; Cassino, F. Roughness and oxidation: Application to NiO growth on Ni at 800 °C. *Mater. Sci. Eng. A* **2000**, *290*, 190–197. [CrossRef]

25. Haugsrud, R. High-temperature oxidation of Cu-10 wt% Ni and Cu-15 wt% Ni at 900–1050 °C. *Corros. Sci.* **2000**, *42*, 383–399. [CrossRef]

26. Evans, J.L. Effect of Surface Roughness on the Oxidation Behavior of the Ni-Base Superalloy ME3. *J. Mater. Eng. Perform.* **2010**, *19*, 1001–1004. [CrossRef]

27. Akhiani, H.; Szpunar, J.A. Effect of surface roughness on the texture and oxidation behavior of Zircaloy-4 cladding tube. *Appl. Surf. Sci.* **2013**, *285*, 832–839. [CrossRef]

28. Weng, F.; Yu, H.; Chen, C.; Wan, K. High-temperature oxidation behavior of Ni-based superalloys with Nb and Y and the interface characteristics of oxidation scales. *Surf. Interface Anal.* **2014**, *47*, 362–370. [CrossRef]

29. Li, W.; Lei, Z.; Shi, X.; Wang, S.; Zhang, Y.; Fan, D. Effect of microgroove surface on surface properties and cytocompatibility of silicone rubber. *J. Third Milit. Med. Univ.* **2015**, *8*, 736–740.

30. Wang, L.; Jiang, W.G.; Li, X.W.; Dong, J.; Zheng, W.; Feng, H.; Lou, L. Effect of Surface Roughness on the Oxidation Behavior of a Directionally Solidified Ni-Based Superalloy at 1100 °C. *Acta Metall. Sin.* **2015**, *28*, 381–385. [CrossRef]

31. Zhang, Z.G.; Hou, P.Y.; Gesmundo, F.; Niu, F. Effect of surface roughness on the development of protective Al_2O_3 on Fe–10Al (at.%) alloys containing 0–10 at.% Cr. *Appl. Surf. Sci.* **2006**, *253*, 881–888. [CrossRef]

32. Qiu, J.; Liu, L.H.; Hsu, P.F. Oxide-Film Effect on Infrared Radiative Properties of Grating Structures of Aluminum. *J. Thermophys. Heat Transf.* **2011**, *25*, 80–86. [CrossRef]

33. Peraldi, R.; Monceau, D.; Pieraggi, B. Correlations between growth kinetics and microstructure for scales formed by high-temperature oxidation of pure nickel. I. morphologies and microstructures. *Oxid. Met.* **2002**, *58*, 249–273. [CrossRef]